A Quantitative Prediction Method for Fracture Density Based on the Equivalent Medium Theory

Liang Sun [1,2], Suping Peng [1,2]*, Dengke He [1,2], Shu Wang [1,2]

[1] State Key Laboratory of Coal Resources and Safe Mining, China University of Mining and Technology (Beijing), Haidian, Beijing 100083, China; yksunliang@163.com (L.S.); He_dengke@126.com (D.H.); sapphiry@icloud.com (S.W.)
[2] College of Geoscience and Surveying Engineering, China University of Mining and Technology (Beijing), Haidian, Beijing 100083, China
* Correspondence: psp@cumtb.edu.cn

Abstract: Fracture density, a critical parameter of unconventional reservoirs, can be used to evaluate potential of unconventional reservoirs and location of production wells. Many technologies, such as amplitude variation with offset and azimuth (AVOA) technology, vertical seismic profiling (VSP) technology, and multicomponent seismic technology, are generally used to predict fracture of reservoirs. they can qualitatively predict fracture by analyzing seismic attributes, including seismic wave amplitudes, seismic wave velocities, which are sensitive to fracture. However, it is important to quantitatively describe fracture of reservoirs. In this study, based on a double-layer model, the relationships between fracture density and the double-layer model's physical parameters, such as velocity of fast shear-wave, velocity of slow shear-wave, and density, were established, and then a powerful quantitative prediction method for fracture density was proposed dramatically. Afterwards, the Hudson model for crack was used to test the applicability of the method. The result shown that the quantitative prediction method for fracture density can be applied suitable to the Hudson model for crack. Finally, the result of validation models indicated that the method can predict fracture density effective, in which absolute relative deviation (ARD) were less than 5% and root-mean-square error (RMSE) was 4.88×10^{-3}.

Keywords: Fracture density; Double-layer model; Unconventional reservoirs; Multicomponent seismic; Shear-wave splitting

1. Introduction

Unconventional resources have received widespread interest in recent years because of their emergence as a source of clean energy, and they are now being developed and produced in North American shales, Southern North China shales, etc. [1-3]. As self-sourced reservoirs, the fracture space controls not only the potential of unconventional reservoirs but also location of production wells [4]. Thus, the accurate prediction of fracture density plays an important role in the exploration and development of unconventional reservoirs. In particular, knowing the fracture density variation between zones within a reservoir can help in the accurate determination of well locations [5].

Many achievements have been made with the continuous improvements by researchers for predicting the fracture in sedimentary strata [6-9]. Sedimentary strata, such as unconventional reservoirs, are usually described as anisotropic mediums on the scale of seismic waves, and the anisotropy of a medium is produced by skeleton orientated arrangement and fracture development [10-11]. Ruger (1997, 2002) researched the relationship among P-wave reflection coefficients, offset, and azimuth named AVOA technology, which was found to be suitable for analyzing the anisotropy of a medium [12-13]. While, some researchers used the AVOA technology to predict the anisotropy of fractured reservoirs for analyzing the fracture development, and the results in these studies were presented by anisotropic parameters to reflect the fracture development [9, 13-15]. Thus, the AVOA technology was a non-direct way to predict the fracture development of reservoirs clearly.

Using the vertical seismic profiling (VSP) technology to predict the fracture development of reservoirs is realized by the splitting property of the S-wave, the S-wave split into fast S-wave and slow S-wave when passing through fracture with an angle [16-17], which is obviously different from AVOA technology. The difference between the velocities of these waves can be estimated by measuring the increase of the time delay between them with the depth [18]. Meadows et al. [19], Pevzner et al. [20], and Shevchenko et al. [21] used VSP technology to predict the fracture of reservoirs. The prediction results shown that the VSP technology can estimate the S-wave anisotropy of reservoirs by the difference between the fast S-wave velocity and the slow S-wave velocity, which was useful for representing the fracture development of reservoirs. However, this technology requires a borehole that is available for the exploration area. Thus, it only has the ability to reflect the fracture development near the borehole, actually. Ata et al. [22], Gaiser [23] and Vetri et al. [24] used multicomponent seismic technology to predict the fracture development of reservoirs by S-wave splitting property. Compare with the VSP technology, multicomponent seismic data did not have the advantage of recording data near the reservoirs, which can bypass complications introduced by the overburden. Fortunately, with the improvement of multicomponent seismic data acquisition and processing technology [25-31], the application of multicomponent seismic technology has gradually increased, providing favorable technical support for identifying the fracture of reservoirs [32-33]. However, Using the splitting property of the S-wave to predict the fracture of reservoirs is also a non-direct way yet.

During the past few decades, the equivalent medium theory, a method for digitizing rocks, has attracted the attention of many researchers [34-36]. Backus [37] demonstrated that a multilayer transversely isotropic medium was equivalent anisotropic if the wavelength of seismic wave is much larger than the monolayer of the multilayer transversely isotropic medium, and then the equivalent elastic tensor of this medium was given. Eshelby [38] studied the situation of a single elliptical inclusion in isotropic media, and then Cheng [39] gave the equivalent elastic tensor of the situation. Hudson [40] researched the condition that fracture is represented as a gap or inclusion with a thin coin-shaped ellipsoid, and provided the equivalent elastic tensor. Schoenberg [41] ignored the shape and microstructure of fracture and considered the fracture was an infinitely thin and very soft stratum satisfying the linear sliding boundary condition. While, a linear sliding model was proposed. Subsequently, the equivalent medium theory has been developed and promoted [42-46].

Based on the equivalent medium theory, this study established the relationships among fracture density, multicomponent seismic response, density. As a result, a powerful quantitative prediction method for fracture density was proposed. Furthermore, the applicability of the quantitative prediction method for fracture density was verified by the Hudson model for crack. In this study, Section 2 addresses details to construct a quantitative prediction method for fracture density based on an equivalent medium model. Section 3 verifies the quantitative prediction method for fracture density with the Hudson model for crack. The data to test the proposed method and discussion in this study are presented in Section 4. Finally, conclusions are presented in Section 5.

2. Method Assumptions and Establishment

In this section, firstly, we make some idealized assumptions in order to achieve a powerful method for predicting fracture density. Secondly, the relationships between the fracture density and the physical parameters of target layer, such as fast S-wave velocity, slow S-wave velocity, root mean square (RMS) velocity, and density, are developed under the idealized assumptions. Finally, calculation Eqs. for the fracture density are given in detail, and then a quantitative prediction method for fracture density is established.

2.1 Assumptions

As a result of their genesis, sedimentary strata, such as unconventional reservoirs, can be exhibited in a thin interbedded medium. In this work, we assume that the thin interbedded medium, shown in Fig. 1, is composed of two components: rock skeleton layer (matrix) represented by black in Fig. 1 and rock fracture layer (including filling, water, oil, and gas) denoted by gray in Fig. 1.

Preprints (www.preprints.org) | NOT PEER-REVIEWED | Posted: 16 April 2018 doi:10.20944/preprints201804.0208.v1

Moreover, following assumptions and simplifications are made to generate a practical method for predicting the fracture density which is defined by the volumetric proportion between the fracture layer and the total layer.

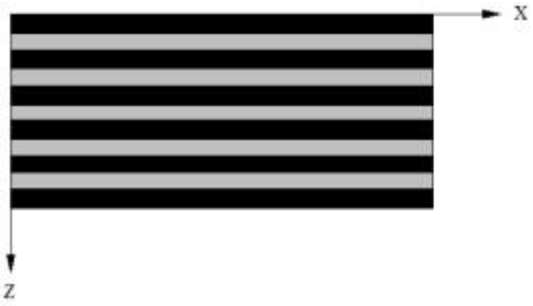

Figure 1. Thin interbedded medium

(1) The rock layer and rock fracture layer of the thin interbedded medium are assumed isotropic, homogeneous, and linear elastic.
(2) There are no sources of intrinsic energy dissipation, such as friction or viscosity, between the rock skeleton layer and the rock fracture layer.
(3) The thickness of the rock skeleton layer and the rock fracture layer must be much smaller than a seismic wavelength, which the seismic wavelength must be at least ten times a layer thickness.

According to the aforementioned assumptions, we can divide the thin interbedded medium into two parts: a skeleton layer and a fracture layer, and then the thin interbedded medium can be equivalent to a double-layer medium. Fig. 2 shows the double-layer medium, in which the black part represents the skeleton layer and the gray part indicates the fracture layer.

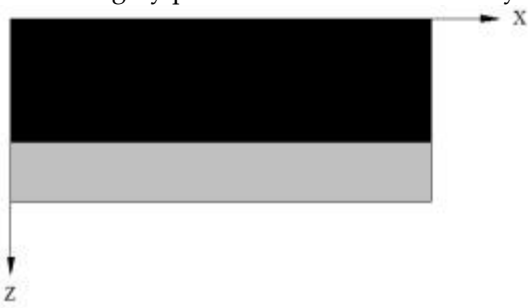

Figure 2. Double-layer medium

2.2 The relationships between S-wave velocities and fracture density

Notable, Backus (1962) demonstrated that if the wavelength of seismic wave is much larger than the monolayer of the thin interbedded medium, it will be equivalent anisotropic [37]. Thus, the stiffness tensor (C) of the double-layer medium can be represented facile by Backus Average, which depicted with the P-wave velocity (V_P), the S-wave velocity (V_S), the density (ρ), and the volume of each layer.

Table 1 Physical parameters of the double-layer medium

	P-wave velocity (m/s)	S-wave velocity (m/s)	Density (kg/m^3)	Volume (m^3)
Skeleton layer	V_{P1}	V_{S1}	ρ_1	d_1
Fracture layer	V_{P2}	V_{S1}	ρ_2	d_2

Tab. 1 shows the physical parameters of the double-layer medium, and then the stiffness tensor (C) of the double-layer medium can be described through Backus average [37] and Levin formula [47], which has the following form:

Preprints (www.preprints.org) | NOT PEER-REVIEWED | Posted: 16 April 2018 doi:10.20944/preprints201804.0208.v1

$$C = \begin{bmatrix} c_{11} & c_{12} & c_{13} & 0 & 0 & 0 \\ c_{12} & c_{11} & c_{13} & 0 & 0 & 0 \\ c_{13} & c_{13} & c_{33} & 0 & 0 & 0 \\ 0 & 0 & 0 & c_{44} & 0 & 0 \\ 0 & 0 & 0 & 0 & c_{55} & 0 \\ 0 & 0 & 0 & 0 & 0 & c_{66} \end{bmatrix} \quad (1)$$

where $c_{55} = c_{44}$; $c_{66} = 0.5(c_{11} - c_{12})$;

$$\begin{cases} c_{11} = \left\langle 4\rho V_S^2 \left(1 - \frac{V_S^2}{V_P^2}\right) \right\rangle + \left\langle 1 - 2\frac{V_S^2}{V_P^2} \right\rangle^2 \left\langle (\rho V_P^2)^{-1} \right\rangle^{-1} \\ c_{12} = \left\langle 2\rho V_S^2 \left(1 - 2\frac{V_S^2}{V_P^2}\right) \right\rangle + \left\langle 1 - 2\frac{V_S^2}{V_P^2} \right\rangle^2 \left\langle (\rho V_P^2)^{-1} \right\rangle^{-1} \\ c_{13} = \left\langle 1 - 2\frac{V_S^2}{V_P^2} \right\rangle^2 \left\langle (\rho V_P^2)^{-1} \right\rangle^{-1} \\ c_{33} = \left\langle (\rho V_P^2)^{-1} \right\rangle^{-1} \\ c_{44} = \left\langle (\rho V_S^2)^{-1} \right\rangle^{-1} \\ c_{66} = \left\langle \rho V_S^2 \right\rangle \end{cases}$$

The brackets $\langle \cdot \rangle$ indicates averages of the enclosed properties weighted by their volumetric proportions, which is often called the Backus average. As a result, we can represent the fast S-wave velocity (V_{Fast}) and the slow S-wave velocity (V_{Slow}) of the double-layer medium as follows:

$$V_{Fast} = \sqrt{c_{66}/\rho_{all}} = \sqrt{(f_1\rho_1 V_{S1}^2 + f_2\rho_2 V_{S2}^2)/(f_1\rho_1 + f_2\rho_2)} \quad (2)$$

$$V_{Slow} = \sqrt{c_{44}/\rho_{all}} = \sqrt{(f_1/\rho_1 V_{S1}^2 + f_2/\rho_2 V_{S2}^2)^{-1}/(f_1\rho_1 + f_2\rho_2)} \quad (3)$$

where $\rho_{all} = f_1\rho_1 + f_2\rho_2$ denotes the average density, kg/m³; $f_1 = 1 - \varepsilon$ represents the volumetric proportion between the skeleton layer and the total layer with the range (0, 1], dimensionless; $f_2 = \varepsilon$ indicates the volumetric proportion between the fracture layer and the total layer with the range [0, 1), dimensionless; $\varepsilon = d_2/(d_1 + d_2)$ is the fracture density with the range [0, 1), dimensionless.

2.3 The relationships between root mean square (RMS) velocities and fracture density

On the basis of above-mentioned, we can develop the relationships between root mean square (RMS) velocities and the fracture density. In this study, the P-wave RMS velocity ($\overline{V}_P$) in the double-layer medium can be expressed as:

$$\overline{V}_P = \sqrt{\frac{t_1 V_{P1}^2 + t_2 V_{P2}^2}{t_1 + t_2}} \quad (4)$$

Preprints (www.preprints.org) | NOT PEER-REVIEWED | Posted: 16 April 2018 doi:10.20944/preprints201804.0208.v1

where $t_1 = d_1/V_{P1}$ represents the vertical propagation time of P-wave in the skeleton layer, s; $t_2 = d_2/V_{P2}$ denotes the vertical propagation time of P-wave in the fracture layer, s. Moreover, the physical parameters of the skeleton layer and the fracture layer, shown in Table 1, are substituted into Eq. (4), we can obtain:

$$\overline{V}_P = \sqrt{\frac{\frac{d_1}{V_{P1}}V_{P1}^2 + \frac{d_2}{V_{P2}}V_{P2}^2}{\frac{d_1}{V_{P1}} + \frac{d_2}{V_{P2}}}} \tag{5}$$

Through further simplification, the Eq. (5) can be rewritten:

$$\overline{V}_P = \sqrt{\frac{(1/\varepsilon - 1)V_{P1} + V_{P2}}{(1/\varepsilon - 1)/V_{P1} + 1/V_{P2}}} \tag{6}$$

In the same way, the S-wave RMS velocity ($\overline{V}_S$) can be obtained as follows:

$$\overline{V}_S = \sqrt{\frac{(1/\varepsilon - 1)V_{S1} + V_{S2}}{(1/\varepsilon - 1)/V_{S1} + 1/V_{S2}}} \tag{7}$$

2.4 The relationship between P-wave velocity and density

Gardner [48] and Castagna [49] studied the relationship between the P-wave velocity and the density in different lithology, and then determined their relationships. Gardner [48] suggested an empirical relation between the P-wave velocity (V_G) and the density (ρ_G) that represents an average over many rock types:

$$\rho_G \approx 1.741 V_G^{0.25} \tag{8}$$

where V_G is in km/s and ρ_G is in g/cm^3, or

$$\rho_G \approx 0.23 V_G^{0.25} \tag{9}$$

where V_G is in ft/s.

2.5 The quantitative prediction method of fracture density

Through aforementioned Eqs. on the relationships between the fracture density and the physical parameters of the double-layer medium, such as the fast S-wave velocity, the slow S-wave velocity, the root mean square (RMS) velocity, and the density, the key issue required to be solved is how to establish a practical method for predicting fracture density.

After the analysis on the correlations of the Eqs. above, we consider to build the relationship between the P-wave velocity and density of a target layer firstly, which is according to the studies by Gardner [48] and Castagna [49]. Actually speaking, a certain amount of core analysis and logging data will be finished before development of an unconventional reservoir, and as a result the non-linear relationships between the P-wave velocity and the density of the target layer can be obtained:

$$\rho_1 = aV_{P1}^{0.25} \tag{10}$$

$$\rho_2 = bV_{P2}^{0.25} \tag{11}$$

Preprints (www.preprints.org) | NOT PEER-REVIEWED | Posted: 16 April 2018 doi:10.20944/preprints201804.0208.v1

where coefficient a reflects the relationship between the P-wave velocity and the density of the skeleton layer, dimensionless; coefficient b indicates the relationship between the P-wave velocity and the density of the fracture layer, dimensionless. Meanwhile, the average density (ρ_{all}) of the target layer can also be obtained:

$$\rho_{all} = f_1\rho_1 + f_2\rho_2 \tag{12}$$

Furthermore, taking Eq. (10) and Eq. (11) into Eq. (6), and its expression Eq. was as follows:

$$\bar{V}_P = \sqrt{\frac{(1/\varepsilon - 1)(\rho_1/a)^4 + (\rho_2/b)^4}{(1/\varepsilon - 1)/(\rho_1/a)^4 + 1/(\rho_2/b)^4}} \tag{13}$$

Notable, the RMS velocities about the P-wave and S-wave, and the velocities about the fast S-wave and the slow S-wave of the prospecting stratum are acquired from a conventional data processing of multicomponent seismic exploration. Moreover, the average density can be obtained from the core analysis and logging data of survey area. Finally, the fracture density can be achieved through solving the Eq. (2), Eq. (3), Eq. (7), Eq. (12), and Eq. (13), and the flowchart of the calculation is illustrated in Fig. 3. According to the aforementioned analysis, we established the quantitative prediction method of fracture density for the first time in this way.

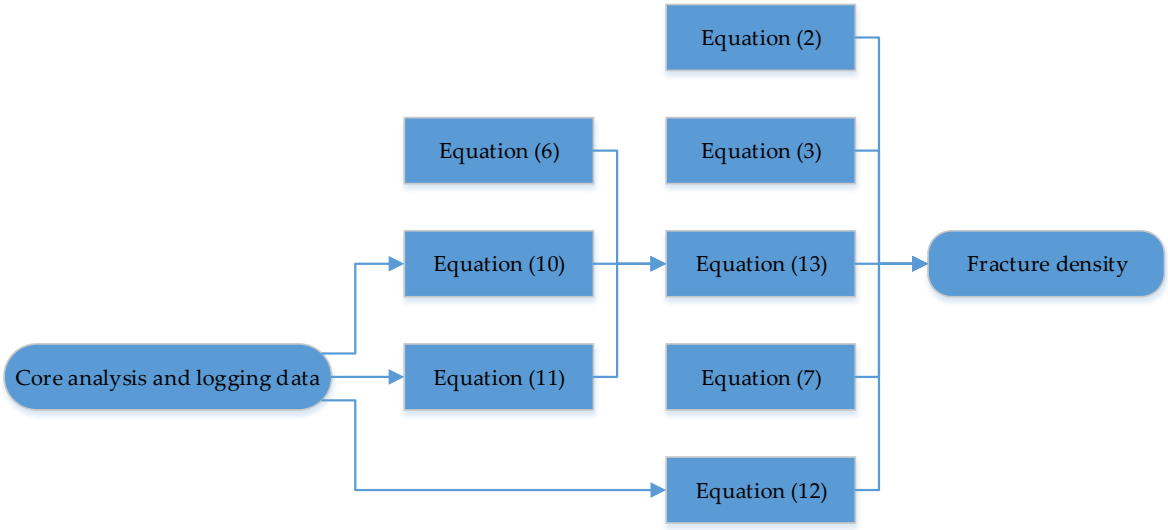

Figure 3 Flowchart of the calculation

3. Application in Hudson Model for Crack

3.1 The quantitative prediction method of fracture density application analysis in Hudson Model for crack

The quantitative method above assumed that a sedimentary stratum consisted of a layered skeleton and a layered fracture. However, fractured strata are often depicted with the Hudson model in seismic prospecting [40], in which the fracture is represented as a gap or inclusion with a thin coin-shaped ellipsoid. It is feasible to predict the fracture density about the Hudson model by the new method if the velocities about the fast S-wave and slow S-wave are acquired from the seismic data processing and the RMS velocities about the P-wave and S-wave can be converted by some skills. Actually speaking, the velocity group consisted of the four velocities above is just the seismic responses about the given model, including the Hudson model and the other equivalent models, which is the concrete links for predicting the fracture density about the Hudson model by the new method based on the double-layer model. The stiffness tensor is the essential factor for the seismic responses. Therefore, the new method can predict the fracture density of the Hudson model if the parameters about the double-layer model can be determined by the stiffness tensor of the Hudson model according to the Eq. (1), which can deduce the RMS velocities about the P-wave and S-wave. The key for applying and verifying the new method to the Hudson model is how to represent the Eq. (1) of the double-layer model by the Hudson model parameters. The section will discuss how to solve

Preprints (www.preprints.org) | NOT PEER-REVIEWED | Posted: 16 April 2018 doi:10.20944/preprints201804.0208.v1

the velocities about the double-layer model by the Hudson model parameters according to the Eq. (1).

Figure 4. Hudson model for crack

Fig. 4 represents the Hudson model, in which black denotes the skeleton part and gray indicates the fracture part. The physical parameters of the Hudson model are shown in Tab. 2, including the P-wave velocity, the S-wave velocity, the density, and the volume of each part, which can depict the stiffness tensor of the Hudson model at any crack width ratio (α^H). Meanwhile, the fracture density (ε) is also defined by the volumetric proportion between the fracture part and the total part.

Table 2 Physical parameters of the Hudson model for crack

	P-wave velocity (m/s)	S-wave velocity (m/s)	Density (kg/m³)	Volume (m³)
Skeleton part	V_{P1}^H	V_{S1}^H	ρ_1^H	d_1^H
Fracture part	V_{P2}^H	V_{S2}^H	ρ_2^H	d_2^H

According to above analysis, we consider that the ρ_1, ρ_2, and ε of the double-layer model are equal to ρ_1^H, ρ_2^H, and ε^H of the Hudson model, respectively. By adjusting the V_{P1}, V_{S1}, V_{P2}, and V_{S2} to make the stiffness tensor of the double-layer model equals to the stiffness tensor of the Hudson model, and then the equivalent RMS velocities about the P-wave and S-wave of the Hudson model can be obtained, which is the key for applying and verifying the new method to the Hudson model. As a result, the above issue is converted to another form that is whether an unique solution set of the V_{P1}, V_{S1}, V_{P2}, and V_{S2} is existence to make the stiffness tensor of the double-layer model equal to the stiffness tensor of the Hudson model.

3.2 Unique solution set determination

In order to obtain the unique solution set of the V_{P1}, V_{S1}, V_{P2}, and V_{S2}, the components of the stiffness tensor (c_{13}, c_{33}, c_{44}, c_{66}) of the double-layer model are used to represent the components of the stiffness tensor (c_{13}^H, c_{33}^H, c_{44}^H, c_{66}^H) of the Hudson model, respectively, which is as follows:

$$\begin{aligned} c_{13}^H &= c_{13} = \left\langle \left(\rho V_P^2\right)^{-1} \right\rangle^{-1} \\ c_{33}^H &= c_{33} = \left\langle 1 - 2\frac{V_S^2}{V_P^2} \right\rangle \left\langle \left(\rho V_P^2\right)^{-1} \right\rangle^{-1} \\ c_{44}^H &= c_{44} = \left\langle \left(\rho V_S^2\right)^{-1} \right\rangle^{-1} \\ c_{66}^H &= c_{66} = \left\langle \rho V_S^2 \right\rangle \end{aligned} \tag{14}$$

The Eqs. (14) can be expanded into the following expression:

$$\begin{aligned}
&\frac{1}{c_{13}^H} = \frac{f_1}{\rho_1 V_{P1}^2} + \frac{f_2}{\rho_2 V_{P2}^2} \\
&\frac{c_{13}^H}{c_{33}^H} = f_1(1-2\frac{V_{S1}^2}{V_{P1}^2}) + f_2(1-2\frac{V_{S2}^2}{V_{P2}^2}) \\
&\frac{1}{c_{44}^H} = \frac{f_1}{\rho_1 V_{S1}^2} + \frac{f_2}{\rho_2 V_{S2}^2} \\
&c_{66}^H = f_1\rho_1 V_{S1}^2 + f_2\rho_2 V_{S2}^2
\end{aligned} \tag{15}$$

For further simplification, we have defined some intermediate variables shown in Eqs. (17), and then Eqs. (15) can be rewritten:

$$\begin{aligned}
y_1 &= a_1 P_1 + a_2 P_2 \\
y_2 &= 1 - 2 f_1 S_1 P_1 - 2 f_2 S_2 P_2 \\
y_3 &= \frac{a_1}{S_1} + \frac{a_2}{S_2} \\
y_4 &= b_1 S_1 + b_2 S_2
\end{aligned} \tag{16}$$

where

$$y_1 = \frac{1}{c_{13}^H} \ , \ y_2 = \frac{c_{13}^H}{c_{33}^H} \ , \ y_3 = \frac{1}{c_{44}^H} \ , \ y_4 = c_{66}^H$$

$$a_1 = \frac{f_1}{\rho_1} \ , \ a_2 = \frac{f_2}{\rho_2} \ , \ b_1 = f_1\rho_1 \ , \ b_2 = f_2\rho_2 \tag{17}$$

$$P_1 = \frac{1}{V_{P1}^2}, \ P_2 = \frac{1}{V_{P2}^2}, \ S_1 = V_{S1}^2, \ S_2 = V_{S2}^2$$

There are two sets of solutions about the variables including the S_1, S_2, P_1, and P_2 which has a certain relation with the V_{P1}, V_{S1}, V_{P2}, and V_{S2}, respectively, through solving the Eqs. (16), and its expressions are as follows:

$$\begin{cases}
S_{1'} = \dfrac{y_4 + \dfrac{1}{2y_3}(a_1b_1 - a_2b_2 - y_3y_4 - (a_1^2b_1^2 - 2a_1a_2b_1b_2 - 2a_1b_1y_3y_4 + a_2^2b_2^2 - 2a_2b_2y_3y_4 + y_3^2y_4^2)^{1/2})}{b_1} \\
S_{2'} = \dfrac{a_2b_2 - a_1b_1 + y_3y_4 + (a_1^2b_1^2 - 2a_1a_2b_1b_2 - 2a_1b_1y_3y_4 + a_2^2b_2^2 - 2a_2b_2y_3y_4 + y_3^2y_4^2)^{1/2}}{2b_2y_3} \\
P_{1'} = -\dfrac{a_2y_2 - a_2 + 2f_2S_{2'}y_1}{2(a_2f_1S_{1'} - a_1f_2S_{2'})} \\
P_{2'} = \dfrac{a_1y_2 - a_1 + 2f_1S_{1'}y_1}{2(a_2f_1S_{1'} - a_1f_2S_{2'})}
\end{cases} \tag{18}$$

Preprints (www.preprints.org) | NOT PEER-REVIEWED | Posted: 16 April 2018 doi:10.20944/preprints201804.0208.v1

$$\begin{cases} S_{1^*} = \dfrac{y_4 + \dfrac{1}{2y_3}(a_1b_1 - a_2b_2 - y_3y_4 + (a_1^2b_1^2 - 2a_1a_2b_1b_2 - 2a_1b_1y_3y_4 + a_2^2b_2^2 - 2a_2b_2y_3y_4 + y_3^2y_4^2)^{1/2})}{b_1} \\ S_{2^*} = \dfrac{a_2b_2 - a_1b_1 + y_3y_4 - (a_1^2b_1^2 - 2a_1a_2b_1b_2 - 2a_1b_1y_3y_4 + a_2^2b_2^2 - 2a_2b_2y_3y_4 + y_3^2y_4^2)^{1/2}}{2b_2y_3} \\ P_{1^*} = -\dfrac{a_2y_2 - a_2 + 2f_2S_{2^*}y_1}{2(a_2f_1S_{1^*} - a_1f_2S_{2^*})} \\ P_{2^*} = \dfrac{a_1y_2 - a_1 + 2f_1S_{1^*}y_1}{2(a_2f_1S_{1^*} - a_1f_2S_{2^*})} \end{cases} \tag{19}$$

where apostrophe denotes the first set of solutions; asterisk represents the other set of solutions. Substituting Eqs. (17) into Eqs. (18) and Eqs. (19), we can obtain:

$$\begin{cases} V_{S1'}^2 = \dfrac{c_{66}^H - \frac{1}{2}c_{44}^H(f_2^2 - f_1^2 + \frac{c_{66}^H}{c_{44}^H} + ((\frac{c_{66}^H}{c_{44}^H})^2 - 2(f_1^2 + f_2^2)\frac{c_{66}^H}{c_{44}^H} + (f_1^2 - f_2^2)^2)^{1/2})}{f_1\rho_1} \\ V_{S2'}^2 = \dfrac{\frac{1}{2}c_{44}^H(f_2^2 - f_1^2 + \frac{c_{66}^H}{c_{44}^H} + ((\frac{c_{66}^H}{c_{44}^H})^2 - 2(f_1^2 + f_2^2)\frac{c_{66}^H}{c_{44}^H} + (f_1^2 - f_2^2)^2)^{1/2})}{f_2\rho_2} \\ V_{P1'}^2 = -\dfrac{2(f_1f_2V_{S1'}^2/\rho_2 - f_1f_2V_{S2'}^2/\rho_1)}{f_2c_{13}^H/\rho_2c_{33}^H - f_2/\rho_2 + 2f_2V_{S2'}^2/c_{33}^H} \\ V_{P2'}^2 = \dfrac{2(f_1f_2V_{S1'}^2/\rho_2 - f_1f_2V_{S2'}^2/\rho_1)}{f_1c_{13}^H/\rho_1c_{33}^H - f_1/\rho_1 + 2f_1V_{S1'}^2/c_{33}^H} \end{cases} \tag{20}$$

$$\begin{cases} V_{S1^*}^2 = \dfrac{c_{66}^H + \frac{1}{2}c_{44}^H(f_1^2 - f_2^2 - \frac{c_{66}^H}{c_{44}^H} + ((\frac{c_{66}^H}{c_{44}^H})^2 - 2(f_1^2 + f_2^2)\frac{c_{66}^H}{c_{44}^H} + (f_1^2 - f_2^2)^2)^{1/2})}{f_1\rho_1} \\ V_{S2^*}^2 = \dfrac{-\frac{1}{2}c_{44}^H(f_1^2 - f_2^2 - \frac{c_{66}^H}{c_{44}^H} + ((\frac{c_{66}^H}{c_{44}^H})^2 - 2(f_1^2 + f_2^2)\frac{c_{66}^H}{c_{44}^H} + (f_1^2 - f_2^2)^2)^{1/2})}{f_2\rho_2} \\ V_{P1^*}^2 = -\dfrac{2(f_1f_2V_{S1^*}^2/\rho_2 - f_1f_2V_{S2^*}^2/\rho_1)}{f_2c_{13}^H/\rho_2c_{33}^H - f_2/\rho_2 + 2f_2V_{S2^*}^2/c_{33}^H} \\ V_{P2^*}^2 = \dfrac{2(f_1f_2V_{S1^*}^2/\rho_2 - f_1f_2V_{S2^*}^2/\rho_1)}{f_1c_{13}^H/\rho_1c_{33}^H - f_1/\rho_1 + 2f_1V_{S1^*}^2/c_{33}^H} \end{cases} \tag{21}$$

According to the Appendix A, Eqs. (20) is not the reasonable solution for the V_{S1}^2, V_{S2}^2, V_{P1}^2, and V_{P2}^2 under the requirement that the S-wave velocity of the skeleton part (V_{S1}^2) should be larger than the S-wave velocity of the fracture part (V_{S2}^2) in the actual situation. Hence, the Eqs. (21) is the

Preprints (www.preprints.org) | NOT PEER-REVIEWED | Posted: 16 April 2018 doi:10.20944/preprints201804.0208.v1

only solution for the V_{S1}^2, V_{S2}^2, V_{P1}^2, and V_{P2}^2. Moreover, it is obviously that there will be have 16 sets of solutions for the V_{S1}, V_{S2}, V_{P1}, and V_{P2}, due to the four parameters at the left of the Eqs. (21) are quadratic. Finally, the Eqs. (22) is the only solution about the Eqs. (21) with the positive number, owing to the other solutions are eliminated under the actual situation that the seismic wave velocities （V_{S1}, V_{S2}, V_{P1}, V_{P2}）must be real numbers larger than zero, which is as follows:

$$\begin{cases} V_{S1^*} = \sqrt{\dfrac{c_{66}^H + \frac{1}{2}c_{44}^H(f_1^2 - f_2^2 - \frac{c_{66}^H}{c_{44}^H} + ((\frac{c_{66}^H}{c_{44}^H})^2 - 2(f_1^2 + f_2^2)\frac{c_{66}^H}{c_{44}^H} + (f_1^2 - f_2^2)^2)^{1/2})}{f_1\rho_1}} \\ V_{S2^*} = \sqrt{\dfrac{-\frac{1}{2}c_{44}^H(f_1^2 - f_2^2 - \frac{c_{66}^H}{c_{44}^H} + ((\frac{c_{66}^H}{c_{44}^H})^2 - 2(f_1^2 + f_2^2)\frac{c_{66}^H}{c_{44}^H} + (f_1^2 - f_2^2)^2)^{1/2})}{f_2\rho_2}} \\ V_{P1^*} = \sqrt{-\dfrac{2(f_1 f_2 V_{S1^*}^2/\rho_2 - f_1 f_2 V_{S2^*}^2/\rho_1)}{f_2 c_{13}^H/\rho_2 c_{33}^H - f_2/\rho_2 + 2 f_2 V_{S2^*}^2/c_{33}^H}} \\ V_{P2^*} = \sqrt{\dfrac{2(f_1 f_2 V_{S1^*}^2/\rho_2 - f_1 f_2 V_{S2^*}^2/\rho_1)}{f_1 c_{13}^H/\rho_1 c_{33}^H - f_1/\rho_1 + 2 f_1 V_{S1^*}^2/c_{33}^H}} \end{cases} \quad (22)$$

Based on the above analysis, there is a set of the P-wave and the S-wave velocities (V_{P1}, V_{P2}, V_{S1}, V_{S2}) that make the stiffness tensor of the double-layer model and the stiffness tensor of the Hudson model equal. Meanwhile, the density of the skeleton part, the density of the fracture part, and the fracture density of the two models are equal. Thus, the quantitative prediction method of fracture density can be applied to the Hudson model.

4. Method Validation and Discussion

4.1 Validation model

In order to examine the effective of the quantitative prediction method of fracture density, ten groups of test models are established to validate the prediction method of fracture density in Tab. 3. Due to the assumptions that the rock skeleton layer and rock fracture layer of a medium are isotropic, homogeneous, and linear elastic, etc. Ten groups of commercial numerical models are performed to validate the application effect of the proposed method in this paper. Each group of test model contains two different core samples. Moreover, the core sample with high velocity and density is defined as a skeleton layer, and the low is defined as a fracture layer, which is conform to the assumptions in Sec. 2.1. As a result, each group of model can be used as a double-layer model. Tab. 3 compiles and condenses the virtually published core samples to establish test models [11,50-51], in which contains the core sample testing conditions and some related materials, including the P-wave velocity (V_P), the S-wave velocity (V_S), the density (ρ) and the fracture density (ε).

Preprints (www.preprints.org) | NOT PEER-REVIEWED | Posted: 16 April 2018 doi:10.20944/preprints201804.0208.v1

Table 3 The core sample parameters of models

Group	Core sample	Conditions	V_P (m/s)	V_S (m/s)	ρ (kg/m^3)	ε
1	Dolomite [51]	P_{eff} = 0 MPa air	5200	2700	2450	0.25
	Shale [51]	P_{eff} = 0 MPa air	2900	1400	2340	
2	Sandy mudstone [50]	P_{eff} = 0 MPa air	4583	2438	2599	0.25
	Mudstone [50]	P_{eff} = 0 MPa air	3619	1920	2629	
3	Mesaverde Mudshale (1949.3m) [11]	P_{eff} = 27.58 MPa Saturated undrained	4529	2703	2520	0.25
	Taylor sandstone [11]	P_{eff} = 0 MPa saturated	3368	1829	2500	
4	Mesaverde immature sandstone(1507.5m) [11]	P_{eff} = 27.58 MPa saturated undrained	4099	2346	2450	0.25
	Taylor sandstone [11]	P_{eff} = 0 MPa saturated	3368	1829	2500	
5	Mesaverde silty limestone(1667.1m) [11]	P_{eff} = 27.58 MPa saturated undrained	4972	2899	2630	0.25
	Taylor sandstone [11]	P_{eff} = 0 MPa saturated	3368	1829	2500	
6	Mesaverde Clayshale (1785.7m) [11]	P_{eff} = 27.58 MPa saturated undrained	3794	2074	2560	0.25
	Taylor sandstone [11]	P_{eff} = 0 MPa saturated	3368	1829	2500	
7	Taylor sandstone [11]	P_{eff} = 0 MPa saturated	3368	1829	2500	0.25
	Dog Creek shale [11]	in situ z=143.3m	1875	826	2000	
8	Taylor sandstone [11]	P_{eff} = 0 MPa saturated	3368	1829	2500	0.25
	Pierre shale [11]	in situ z=450m	2074	869	2250	
9	Oil Shale [11]	unknown	4231	2539	2370	0.25
	Taylor sandstone [11]	P_{eff} = 0 MPa saturated	3368	1829	2500	
10	Taylor sandstone [11]	P_{eff} = 0 MPa saturated	3368	1829	2500	0.25
	Green River shale [11]	P_{eff}=0 MPa saturated undrained	3292	1768	2075	

Abbreviations: P*eff* represents effective stress under triaxial compression; air denotes natural unsaturated state; in situ indicates in-situ measurement.

4.2 Validation model forward

Tab. 3 provides ten groups of model, which are regard as the double-layer model. Thus, the physical parameters of the models can be calculated according to the above Eqs. in Sec. 2. Tab. 4 shows the fast S-wave velocity (V_{Fast}), the slow S-wave velocity (V_{Slow}), the P-wave RMS velocity ($\overline{V}_P$), the S-wave RMS velocity ($\overline{V}_S$), the average density (ρ_{all}), the coefficient *a*, and the coefficient *b*, which are calculated with the Eq. (2), Eq. (3), Eq. (6), Eq. (7), Eq. (12), Eq. (10), and Eq. (11), respectively. Actually speaking, the fast S-wave velocity, slow S-wave velocity, P-wave RMS velocity, S-wave RMS velocity of the prospecting stratum can be obtained from a conventional data processing of multicomponent seismic exploration. In addition, the average density, the coefficient *a*, and the

Preprints (www.preprints.org) | NOT PEER-REVIEWED | Posted: 16 April 2018 doi:10.20944/preprints201804.0208.v1

coefficient b can be achieved from the core analysis and logging data of survey area. Finally, the fracture density (ε) is predicted by the method of fracture density through solving the Eq. (2), Eq. (3), Eq. (7), Eq. (12), and Eq. (13).

Table 4 The physical parameters of models

Group	V_{Fast} (m/s)	V_{Slow} (m/s)	$\overline{V_P}$ (m/s)	$\overline{V_S}$ (m/s)	ρ_{all} (kg/m^3)	a	b
1	2450	2068	4480	2281	2423	1.622	1.793
2	2318	2272	4319	2296	2607	1.776	1.906
3	2514	2373	4204	2449	2515	1.727	1.845
4	2226	2179	3902	2204	2463	1.722	1.845
5	2681	2456	4507	2580	2598	1.761	1.845
6	2017	2002	3683	2010	2545	1.834	1.845
7	1669	1242	2900	1488	2375	1.845	1.709
8	1658	1316	2978	1509	2438	1.845	1.875
9	2375	2296	3996	2338	2402	1.653	1.845
10	1816	1805	3349	1814	2394	1.845	1.541

4.3 Results

According to the quantitative prediction method of fracture density in Sec. 2.5 and the aforementioned physical parameters of models in Tab. 4, we can predict the fracture density (ε). Moreover, we used the quasi-Newton method to solve the Eq. (2), Eq. (3), Eq. (7), Eq. (12), and Eq. (13) for predicting the fracture density in this study. Fig. 5 shows the predicted values of the fracture density (ε'). It can be seen that the predicted fracture density is 0.24–0.25 for the ten models, which indicates the effective of the predicted values for the fracture density. The minimum value located in the seventh model, with a value of about 0.241, and the maximum value, 0.249 is located in the fourth model.

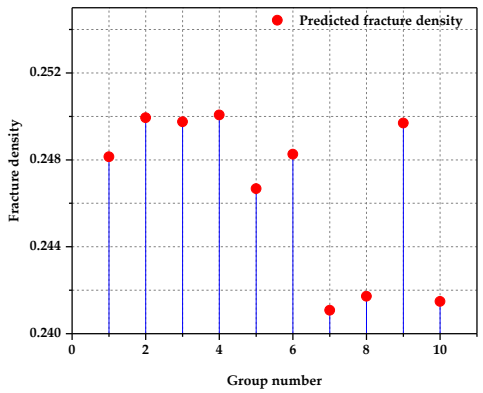

Figure 5. The predicted fracture density.

In addition to the predicted values for the fracture density, the root-mean-square error (RMSE) and absolute relative deviation (ARD) were used as indexes to evaluate the prediction effects. The smaller the root-mean-square (RMSE) and ARD were, the more favorable the prediction effect was. The root-mean-square error (RMSE) was used to weight the deviation between the prediction result and the actual value, and its calculation Eq. was Eq. (23). The ARD was usually used to evaluate the accuracy of method through comparing the prediction value and the actual value. Its calculation Eq. is Eq. (24), as follows:

Preprints (www.preprints.org) | NOT PEER-REVIEWED | Posted: 16 April 2018 doi:10.20944/preprints201804.0208.v1

$$RMSE = \sqrt{\frac{\sum_{i=1}^{n}\left(\varepsilon_i - \varepsilon_i^{'}\right)^2}{n}} \tag{23}$$

$$ARD = \left|\frac{\varepsilon_i - \varepsilon_i^{'}}{\varepsilon_i}\right| \times 100 \quad i = 1, 2, ..., n \tag{24}$$

In Eq. (23) and Eq. (24), $\varepsilon_i^{'}$ represents the prediction fracture density; ε_i denotes the actual fracture density; and n indicates the number of the validation models.

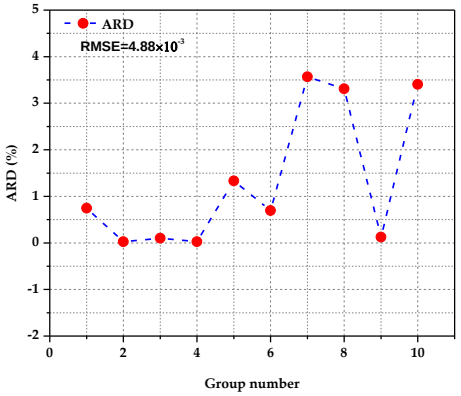

Figure 6. The RMSE and ARD of the predicted fracture density.

Fig. 6 shows the results of RMSE and ARD. It was shown that ARD were less than 5% and RMSE was 4.88×10^{-3}. It indicated that the fracture density predicted by the method developed in this study were in agreement with the actual data. The results demonstrated that the quantitative prediction method proposed in this study was capable for predicting fracture density data.

In this study, for establishing a practical method to predict the fracture density quantitatively, we assume that a thin interbedded medium is composed of two components: rock skeleton layer (matrix) and rock fracture layer (including filling, water, oil, and gas), and the rock skeleton layer and rock fracture layer of the thin interbedded medium are isotropic, homogeneous, and linear elastic, etc., which is an idealized hypothesis. As a result, the thin interbedded medium can equivalent to the double-layer medium under these assumptions. Actually speaking, these assumptions will involve in deviation to this method, and the effect of these assumptions on the prediction method of fracture density will be the focus in the future research. However, it is significant that the new method can provide a scale in predicting the fracture density. Besides, the new method can be applied to the Hudson model, and then the scope of the prediction method of fracture density is extended, which is verified in Sec. 3.

Based on the above assumptions, the relationships between fracture density and the seismic response is established. In Sec. 2.2-2.3, we use the fast S-wave velocity, the slow S-wave velocity, the P-wave RMS velocity, and the S-wave RMS velocity as constraints to predict the fracture density, which can be obtained from a conventional data processing of multicomponent seismic exploration. Therefore, the processing quality of the multicomponent data will affect the application of the prediction method for fracture density. Besides, only concerns the wave velocity as a function of density in Sec. 2.4 is imprecise, which is to simplify the prediction method. In fact, the velocity is related to several factors among which for instance the Young's modulus. Moreover, there will be an error in predicting the average density of a target layer by the core analysis and logging data. The influence of these factors on the prediction results will be reported in the later article.

5. Conclusions

The accurate prediction of fracture density plays an important role in the exploration and development of unconventional reservoirs which have received widespread interest in recent years.

In this study, we considered that a thin interbedded medium is composed of the rock skeleton layer and rock fracture layer, besides the rock skeleton layer and rock fracture layer are isotropic, homogeneous, and linear elastic, etc. Under the above assumptions, the thin interbedded medium can be equivalent to a double-layer medium, and then the relationships between the fracture density and the physical parameters of a target layer, such as the fast S-wave velocity, the slow S-wave velocity, the root mean square (RMS) velocity, and the density, were established, which makes up the gap between the fracture density and the seismic response. While, a quantitative prediction method for fracture density was proposed. Afterwards, the Hudson model was used to test the applicability of this method. The result shown that the new method can be applied to the Hudson model. Moreover, the quantitative prediction method of fracture density was used to the ten groups of validation model, in which RMSE and ARD were as the index of evaluation. The RMSE=4.88×10^{-3} demonstrated that the fracture density predicted by the method developed in this study are in satisfactory agreement with the actual data. Meanwhile, the ARD of the fracture density were less than 5%, which indicated that this method can accurately predict fracture density. All in all, a powerful method for predicting fracture density is proposed in this study, and the method can be used to predict the fracture density of unconventional reservoirs, which provided a new idea for the study of reservoirs fracture.

Acknowledgments: This research is financially supported by the National Science and Technology Supporting Program (2012BAB13B01), National Key Scientific Instrument and Equipment Development Program (2012YQ030126), National Natural Science Foundation of China (41504041).

Author Contributions: Suping Peng was the director of the project. Dengke He proposed the idea of the method. Liang Sun was responsible to build the method, models and write this draft. Shu Wang made some constructive suggestions for the test data.

Conflicts of Interest: The authors declare no conflict of interest.

Nomenclature

a	Coefficient between the P-wave velocity and the density for the skeleton layer (dimensionless)
b	Coefficient between the P-wave velocity and the density for the fracture layer (dimensionless)
C	Stiffness tensor (N/m^2)
C^H	Stiffness tensor of Hudson model (N/m^2)
d_1	Volume of the skeleton (m^3)
d_1^H	Volume of the skeleton in Hudson model (m^3)
d_2	Volume of the fracture (m^3)
d_2^H	Volume of the fracture in Hudson model (m^3)
f_1	Volumetric proportion between the skeleton layer and the total layer (dimensionless)
f_2	Volumetric proportion between the fracture layer and the total layer (dimensionless)
P_{eff}	Effective stress (MPa)
t_1	Vertical propagation time of P-wave in the skeleton layer (s)
t_2	Vertical propagation time of P-wave in the fracture layer (s)
V_{Fast}	Fast S-wave velocity (m/s)
V_G	P-wave velocity in Gardner empirical formula (m/s)
V_P	P-wave velocity (m/s)
$\overline{V_P}$	Root mean square velocity of P-wave (m/s)
V_{P1}	P-wave velocity of the skeleton (m/s)

V_{P1}^{H}	P-wave velocity of the skeleton in Hudson model (m/s)
V_{P2}	P-wave velocity of the fracture (m/s)
V_{P2}^{H}	P-wave velocity of the fracture in Hudson model (m/s)
V_S	S-wave velocity (m/s)
$\overline{V_S}$	Root mean square velocity of S-wave (m/s)
V_{S1}	S-wave velocity of the skeleton (m/s)
V_{S1}^{H}	S-wave velocity of the skeleton in Hudson (m/s)
V_{S2}	S-wave velocity of the fracture (m/s)
V_{S2}^{H}	S-wave velocity of the fracture in Hudson (m/s)
V_{Slow}	Slow S-wave velocity (m/s)

Greek letters

α	Fracture width ratio (dimensionless)
ε	Fracture density (dimensionless)
ε^{H}	Fracture density of Hudson model (dimensionless)
ε'	Prediction value of fracture density (dimensionless)
ρ	Density (Kg/m^3)
ρ_1	Density of the skeleton (Kg/m^3)
ρ_1^{H}	Density of the skeleton in Hudson model (Kg/m^3)
ρ_2	Density of the fracture (Kg/m^3)
ρ_2^{H}	Density of the fracture in Hudson model (Kg/m^3)
ρ_{all}	Average density (Kg/m^3)
ρ_G	Density in Gardner empirical formula (Kg/m^3)

References

1. Montgomery, S.L.; Jarvie D.M.; Bowker, K.A.; Pallastro, R.M. Mississippian Barnett shale, Fort Worthbasin, north-central Texas: Gas-shale play with multitrillion cubic foot potential. *AAPG Bulletin* 2005, 90, 963-966, doi: 10.1306/09170404042.
2. Dang, W.; Zhang, J.C.; Tang, X.; et al. Investigation of gas content of organic-rich shale: A case study from Lower Permian shale in southern North China Basin, central China. *Geoscience Frontiers* 2018, 9, 559-575, doi: 10.1016/j.gsf.2017.05.009.
3. Wang, Y.; Zhu, Y.M.; Liu, Y.; Chen, S.B. Reservoir characteristics of coal-shale sedimentary sequence in coal-bearing strata and their implications for the accumulation of unconventional gas. *Geoscience Frontiers* 2018, 9, 559-575, doi.org/10.1016/j.gsf.2017.05.009. *Journal of Geophysics and Engineering* 2018, 15, 411-420, doi: 10.1088/1742-2140/aa9a10.
4. Wang, X.Z.; Zhang, L.X.; Jiang, C.F.; Fan, B.J. Hydrocarbon storage space within lacustrine gas shale of the Triassic Yanchang Formation, Ordos Basin, China. *Interpretation* 2015, 3, SJ15-SJ23, doi: 10.1190/INT-2014-0125.1.
5. Saidian, M.; Ghazanfari, M.H.; Masihi, M.; Kharrat, R. Five-spot injection/production well location design based on fracture Geometrical Characteristics in Heavy Oil Fractured Reservoirs during Miscible Displacement: An Experimental Approach. *Chemical Engineering Communications* 2012, 199, 306-320, doi: 10.1080/00986445.2011.577849.
6. Johansen, T.A.; Jensen, E.H.; Mavko, G.; Dvorkin, J. Inverse rock physics modeling for reservoir quality prediction. *Geophysics* 2013, 78, M1-M18, doi: 10.1190/GEO2012-0215.1.
7. Far, M.E.; Hardage, B.; Wagner, D. Fracture parameter inversion for Marcellus Shale. *Geophysics* 2014, 79, C55-C63, doi: 10.1190/GEO2013-0236.1.

8. Cui, X.Q.; Krebes, E.; Lines, L.R. Seismic inversion for geologic fractures and fractured media. *Geophysics* 2017, 82, C145-C161, doi: 10.1190/geo2016-0123.1.
9. Fang, X.D.; Zheng, Y.C.; Fehler, M.C. Fracture clustering effect on amplitude variation with offset and azimuth analyses. *Geophysics* 2017, 82, N13-N25, doi: 10.1190/GEO2016-0045.1.
10. Wang, Y.; Zhu, Y.M.; Liu, Y.; Chen, S.B. Reservoir characteristics of coal–shale sedimentary sequence in coal-bearing strata and their implications for the accumulation of unconventional gas. *Journal of Geophysics and Engineering* 2017, 15, 411-420, doi: 10.1088/1742-2140/aa9a10.
11. Thomsen, L. Weak elastic anisotropy. *Geophysics* 1986, 51, 1954-1966, doi: 10.1190/1.1442051.
12. Rüger, A. P-wave reflection coefficients for transversely isotropic models with vertical and horizontal axis of symmetry. *Geophysics* 1997, 62, 713–722, doi: 10.1190/1.1444181.
13. Rüger, A. *Reflection coefficients and azimuthal AVO Analysis in anisotropic media*. Society of Exploration Geophysicists: Tulsa, USA, 2002, ISBN 0-931830-56-7.
14. Mallick, S.; Craft, K.L.; Meister, L.J.; Chambers, R.E. Determination of the principal directions of azimuthal anisotropy from P-wave seismic data. *Geophysics* 1997, 63, 692-706, doi: 10.1190/1.1444369.
15. Bachrach, R.; Sengupta, M.; Salama, A.; Miller, P. Reconstruction of the layer anisotropic elastic parameters and high-resolution fracture characterization from P-wave data: a case study using seismic inversion and Bayesian rock physics parameter estimation. *Geophysical Prospecting* 2009, 57, 253-262, doi: 10.1111/j.1365-2478.2008.00768. x.
16. Wei, J.X.; Di, B.R.; Wang, C.Y. Experiment observation of torsion wave splitting in anisotropic medium. *Chinese Journal of Geophysics* 2006, 49, 1755-1761, doi: 10.1002/cjg2.987.
17. Tang, C.H.; Rial, J.A.; Lees, J.M. Observations and analyses of shear wave splitting in the geothermal field at Hengill, Iceland. *Seismological Research Letters* 2015, 86, 424-430, doi: 10.1785/0220190099
18. Crampin, S. Evaluation of anisotropy by shear-wave splitting. *Geophysics* 1985, 50, 142-152, doi: 10.1190/1.1441824.
19. Meadows, M.A.; Winterstein, D.F. Seismic detection of a hydraulic fracture from shear-wave VSP data at Lost Hills Field, California. *Geophysics* 1994, 59, 11-26, doi: 10.1190/1.1443523.
20. Pevzner, R.; Gurevich, B.; Urosevic, M. Estimation of azimuthal anisotropy from VSP data using multicomponent S-wave velocity analysis. *Geophysics* 2011, 76, D2-D9, doi: 10.1190/geo2010-0290.1.
21. Shevchenko, S.; Tcherkashnev, S.; Kuznetsov, M.; Mamleef, T. Mapping of fracture zones and small faults using VSP and Cross Dipole Sonic in Eastern Siberia Carbonate Reservoirs, Yurubchansky Field, Russia. 25th ASEG Conference and Exhibition, Adelaide, Australia, 2016.
22. Ata, E.; Michelena, R.J. Mapping distribution of fractures in a reservoir with P-S converted waves. *The leading Edge* 1995, 14, 664-676, doi: 10.1190/1.1437141.
23. Gaiser, J.E. Applications for vector coordinate systems of 3-D converted-wave data. *The Leading Edge* 1999, 18, 1290-1300, doi: 10.1190/1.1438202.
24. Vetri, L.; Loinger, E.; Gaiser, J.; et al. 3D/4C Emilio: Azimuth processing and anisotropy analysis in a fractured carbonate reservoir. *The Leading Edge* 2003, 22, 675–679, doi: 10.1190/1.1599695.
25. Peng, S.P.; He, D.K.; Gou, J.W.; Liu, W.J. Binning and fold calculation for converted-wave survey. *Journal of China Coal Society* 2008, 33, 55-58, doi: 10.13225/j.cnki.jccs.2008.02.012.
26. He, D.K.; Peng, S.P.; Sun, L. A Static correction method based on common attitude gathers. *Chinese Journal of Geophysics* 2018, 61, 258-266, doi: 10.6038/cjg2018K0527.
27. Yuan, C.F.; Peng, S.P.; Yang, L.L. An exact solution of the coordinate equation of the conversion point for P-SV converted waves at a horizontal reflector. *Chinese Journal of Geophysics* 2005, 48, 1179-1184, doi: 10.1002/cjg2.772.
28. Huang, Z.Y.; Zhao, J.Z. Technique of S-wave splitting detection by orthonormal basis rotation. *Oil Geophysicsl Prospecting* 2004, 39, 149-152, doi: 10.13810/j.cnki.issn.1000-7210.2004.02.005.
29. Dariu, H.P.; Granger, Y. Birefringence analysis using simulated annealing. Expanded Abstract of 67th EAGE Annual Conference, Madrid, Spain, 2005; Z99.
30. Dewangan, P.; Tsvankin, I. Velocity-independent layer stripping of PP and PS reflection traveltimes. *Geophysics* 2006, 71, U59-U65, doi: 10.1190/1.2369729.
31. Wang, X.; Tsvankin, I. Estimation of interval anisotropy parameters using velocity independent layer stripping. *Geophysics* 2009, 27, WB117-WB127, doi: 10.1190/1.3063981.

32. Bale, R.; Gratakos, B.; Mattocks, B.; Lil, X. Shear wave splitting applications for fracture analysis and improved imaging: some onshore examples. *First Break* 2009, 27, 73-83, www.cgg.com/technicalDocuments/cggv_0000008753.pdf.
33. Lu, J.; Meng, X.H.; Wang, Y.; Yang, Z. Prediction of coal seam details and mining safety using multicomponent seismic data: A case history from China. *Geophysics* 2016, 81, B149-B165, doi: 10.1190/geo2016-0009.1.
34. Kuster, G.Y. Velocity and attenuation of seismic waves in two-phase media: Part I. Theoretical formulations. *Geophysics* 1974, 39, 587-606, doi: 10.1190/1.1440450.
35. Norris, A.N. A differential scheme for the effective moduli of composites. *Mechanics of Materials* 1985, 4, 1-16, doi: 10.1016/0167-6636(85)90002-X.
36. Sayar, P.; Carlos, T.V. Using anisotropic effective medium theories to quantify elastic properties of sandstone-shale laminated rocks. *Geophysics* 2016, 81, D315-D333, doi: 10.1190/geo2015-0323.1.
37. Backus, G.E. Long-wave elastic anisotropy produced by horizontal layering. *Journal of Geophysical Research* 1962, 67, 4427–4440, doi: 10.1029/JZ067i011p04427.
38. Eshelby, J.D. The determination of the elastic field of an ellipsoidal inclusion, and related problems. *Proceedings of the Royal Society of London* 1957, 241, 376-396, doi: 10.1098/rspa.1957.0133.
39. Cheng, C.H. Crack models for a transversely anisotropic medium. *Journal of Geophysical Research Atmospheres* 1993, 98, 675-684, doi: 10.1029/92JB02118.
40. Hudson, J.A. Overall properties of a cracked solid. *Math. Proc. Camb. Phil. Soc.* 1980, 88, 371-384, doi: 10.1017/S0305004100057674.
41. Schoenberg, M. Elastic wave behavior across linear slip interfaces. *Journal of Acoustical Society of America* 1998, 68, 1516-1521, doi: 10.1121/1.385077.
42. Crampin S. A review of wave motion in anisotropic and cracked elastic media. *Wave Motion* 1981, 40, 343-391, doi: 10.1016/0165-2125(81)90026-3.
43. Liu, E.R.; Zeng, X.W. Effective elastic constant of fractured medium. *Oil Geophysical Prospecting* 2001, 36, 38-441, doi: 10.13810/j.cnki.issn.1000-7210.2001.01.007.
44. Budarapu, P.R.; Gracie, R.; Yang, S.W.; Rabczuk, T. Efficient coarse graining in multiscale modeling of fracture. *Theoretical and Applied Fracture Mechanics* 2014, 69, 126-143, doi: 10.1016/j.tafmec.2013.12.004
45. Budarapu, P.R.; Gracie, R.; Bordas, S.P.A.; Rabczuk, T. An adaptive multiscale method for quasi-static crack growth. *Computational Mechanics* 2014, 53, 1129-1148, doi: 10.1007/s00466-013-0952-6.
46. Talebi, H.; Silani, M.; Rabczuk, T. Concurrent multiscale modeling of three dimensional crack and dislocation propagation. *Advances in Engineering Software* 2015, 80, 82-92, doi: 10.1016/j.advengsoft.2014.09.016.
47. Levin, F.K. Seismic velocities in transversely isotropic media. *Geophysics* 1979, 44, 918-936, doi: 10.1190/1.1440985.
48. Gardner, G.H.F.; Gardner, L.W.; Gardner, A.R. Formation velocity and density-The diagnostic basics for stratigraphic trap. *Geophysics* 1974, 39, 770-780, doi: 10.1190/1.1440465.
49. Castagna, J.P.; Batzle, M.L.; Kan, T.K. *Rock physics-The link between rock properties and AVO response*, Society of Exploration Geophysicists: Tulsa, USA, 1993; 8, pp. 135-171, ISBN 093183046X.
50. Dong, S.H. Evaluation technique of azimuthal anisotropic cracks from P wave data and test of elastic anisotropic coefficients of coal. *Ph.D. thesis* 2004, China University of Mining and Technology.
51. Mavko, G.; Mukerji, T.; Dvorkin, J. *Tools for seismic analysis in porous media*, Cambridge University Press: Cambridge, UK, 1998, pp. 142-146, ISBN 0-521-62068-6.

Appendix A

The difference between $V_{S1'}^2$ and $V_{S2'}^2$ in Eqs. (20) represented as $g = V_{S2'}^2 - V_{S1'}^2$. And the following process will check up the range, larger or less than zero, of the g. The g can be can be expanded into the following expression:

Preprints (www.preprints.org) | NOT PEER-REVIEWED | Posted: 16 April 2018 doi:10.20944/preprints201804.0208.v1

$$g = \frac{\frac{1}{2}c_{44}^H(f_2^2 - f_1^2 + \frac{c_{66}^H}{c_{44}^H} + ((\frac{c_{66}^H}{c_{44}^H})^2 - 2(f_1^2 + f_2^2)\frac{c_{66}^H}{c_{44}^H} + (f_1^2 - f_2^2)^2)^{1/2})}{f_2\rho_2} - \frac{c_{66}^H - \frac{1}{2}c_{44}^H(f_2^2 - f_1^2 + \frac{c_{66}^H}{c_{44}^H} + ((\frac{c_{66}^H}{c_{44}^H})^2 - 2(f_1^2 + f_2^2)\frac{c_{66}^H}{c_{44}^H} + (f_1^2 - f_2^2)^2)^{1/2})}{f_1\rho_1} \quad (A1)$$

Omitting ρ_1 and ρ_2 ($\rho_1 > \rho_2 > 0$) in Eq. (A1), and then the both sides of Eq. (A1) are divided by $c_{44}^H > 0$:

$$\frac{g}{c_{44}^H} > \frac{\frac{1}{2}(f_2^2 - f_1^2 + \frac{c_{66}^H}{c_{44}^H} + ((\frac{c_{66}^H}{c_{44}^H})^2 - 2(f_1^2 + f_2^2)\frac{c_{66}^H}{c_{44}^H} + (f_1^2 - f_2^2)^2)^{1/2})}{f_2} - \frac{\frac{c_{66}^H}{c_{44}^H} - \frac{1}{2}(f_2^2 - f_1^2 + \frac{c_{66}^H}{c_{44}^H} + ((\frac{c_{66}^H}{c_{44}^H})^2 - 2(f_1^2 + f_2^2)\frac{c_{66}^H}{c_{44}^H} + (f_1^2 - f_2^2)^2)^{1/2})}{f_1} \quad (A2)$$

Multiplying Eq. (A2) by $f_1 f_2 > 0$ in both side, we can obtain:

$$\frac{g}{c_{44}^H} f_1 f_2 > \frac{1}{2} f_1(f_2^2 - f_1^2 + \frac{c_{66}^H}{c_{44}^H} + ((\frac{c_{66}^H}{c_{44}^H})^2 - 2(f_1^2 + f_2^2)\frac{c_{66}^H}{c_{44}^H} + (f_1^2 - f_2^2)^2)^{1/2}) - \left(\frac{c_{66}^H}{c_{44}^H} f_2 - \frac{1}{2} f_2(f_2^2 - f_1^2 + \frac{c_{66}^H}{c_{44}^H} + ((\frac{c_{66}^H}{c_{44}^H})^2 - 2(f_1^2 + f_2^2)\frac{c_{66}^H}{c_{44}^H} + (f_1^2 - f_2^2)^2)^{1/2})\right) \quad (A3)$$

Through further simplification, the Eq. (A3) can be rewritten:

$$\frac{g}{c_{44}^H} f_1 f_2 > \frac{1}{2}(f_1 + f_2)(f_2^2 - f_1^2 + \frac{c_{66}^H}{c_{44}^H} + ((\frac{c_{66}^H}{c_{44}^H})^2 - 2(f_1^2 + f_2^2)\frac{c_{66}^H}{c_{44}^H} + (f_1^2 - f_2^2)^2)^{1/2}) - \frac{c_{66}^H}{c_{44}^H} f_2 \quad (A4)$$

because of $f_1 + f_2 = 1$, the Eq. (A4) can be rewritten:

$$\frac{g}{c_{44}^H} f_1 f_2 > \frac{1}{2}(f_2^2 - f_1^2 + \frac{c_{66}^H}{c_{44}^H} + ((\frac{c_{66}^H}{c_{44}^H})^2 - 2(f_1^2 + f_2^2)\frac{c_{66}^H}{c_{44}^H} + (f_1^2 - f_2^2)^2)^{1/2} - \frac{c_{66}^H}{c_{44}^H} f_2 \quad (A5)$$

Through further simplification, the Eq. (A5) can be rewritten:

$$\frac{g}{c_{44}^H} f_1 f_2 > \left(1 - \frac{c_{66}^H}{c_{44}^H}\right)\left(f_2 - \frac{1}{2}\right) + \frac{1}{2}(((\frac{c_{66}^H}{c_{44}^H})^2 - 2(f_1^2 + f_2^2)\frac{c_{66}^H}{c_{44}^H} + (f_1^2 - f_2^2)^2)^{1/2}) \quad (A6)$$

According to the essential hypothesis of Hudson theory for crack, we can obtain:

$$\frac{c_{66}^H}{c_{44}^H} > 1, \quad f_2 < 0.1, \quad ((\frac{c_{66}^H}{c_{44}^H})^2 - 2(f_1^2 + f_2^2)\frac{c_{66}^H}{c_{44}^H} + (f_1^2 - f_2^2)^2)^{1/2} > 0$$

Preprints (www.preprints.org) | NOT PEER-REVIEWED | Posted: 16 April 2018 doi:10.20944/preprints201804.0208.v1

Notable, The Eq. (A6) is larger than zero, which is as follows:

$$\frac{g}{c_{44}^H} f_1 f_2 > \left(1-\frac{c_{66}^H}{c_{44}^H}\right)\left(f_2-\frac{1}{2}\right)+\frac{1}{2}(((\frac{c_{66}^H}{c_{44}^H})^2-2(f_1^2+f_2^2)\frac{c_{66}^H}{c_{44}^H}+(f_1^2-f_2^2)^2)^{1/2})>0 \quad \text{(A7)}$$

Because of $c_{44}^H > 0$ and $f_1 f_2 > 0$, so that $g = V_{S2'}^2 - V_{S1'}^2 > 0$. However, V_{S1} and V_{S2} are the S-wave velocities about the skeleton part and the fracture part, respectively, according to the actual conditions. Thus $V_{S2'}^2 - V_{S1'}^2 < 0$, as a result, Eqs. (20) is not a reasonable solution.